

# Out-of-Distribution Semantic Occupancy Prediction

Yuheng Zhang<sup>1,\*</sup>, Mengfei Duan<sup>1,\*</sup>, Kunyu Peng<sup>2,3,†</sup>, Yuhang Wang<sup>1</sup>, Ruiping Liu<sup>2</sup>, Fei Teng<sup>1</sup>, Kai Luo<sup>1</sup>, Zhiyong Li<sup>1</sup>, and Kailun Yang<sup>1,4,†</sup>

**Abstract**—3D semantic occupancy prediction is crucial for autonomous driving, providing a dense, semantically rich environmental representation. However, existing methods focus on in-distribution scenes, making them susceptible to Out-of-Distribution (OoD) objects and long-tail distributions, which increases the risk of undetected anomalies and misinterpretations, posing safety hazards. To address these challenges, we introduce Out-of-Distribution Semantic Occupancy Prediction, targeting OoD detection in 3D voxel space. To fill dataset gaps, we propose a Realistic Anomaly Augmentation that injects synthetic anomalies while preserving realistic spatial and occlusion patterns, enabling the creation of two datasets: VAA-KITTI and VAA-KITTI-360. Then, a novel framework that integrates OoD detection into 3D semantic occupancy prediction, OccOoD, is proposed, which uses Cross-Space Semantic Refinement (CSSR) to refine semantic predictions from complementary voxel and BEV representations, improving OoD detection. Experimental results demonstrate that OccOoD achieves state-of-the-art OoD detection with an AuROC of 65.50% and an AuPRC<sub>r</sub> of 31.83% within a 1.2m region, while maintaining competitive semantic occupancy prediction performance and generalization in real-world urban driving scenes. The established datasets and source code will be made publicly available at <https://github.com/7uHeng/OccOoD>.

## I. INTRODUCTION

3D scene understanding is fundamental to autonomous driving, crucial for motion planning and obstacle avoidance [1]. The cost-effectiveness and ease of deployment of cameras have made vision-based 3D understanding methods a focal point of research [2], [3]. Among these methods, 3D semantic occupancy prediction networks [4] are distinguished by their ability to accurately reconstruct geometry and semantic details. By producing detailed occupancy maps with rich semantic context, these networks improve environmental perception and decision-making, enhancing the safety and reliability of autonomous navigation.

However, current methods [5]–[10] primarily focus on in-distribution scenarios, where models are trained and evaluated on predefined semantic distributions and scenes. While

This work was supported in part by the National Natural Science Foundation of China (Grant No. 62473139), in part by the Hunan Provincial Research and Development Project (Grant No. 2025QK3019), and in part by the State Key Laboratory of Autonomous Intelligent Unmanned Systems (the opening project number ZZKF2025-2-10).

<sup>1</sup>The authors are with the School of Artificial Intelligence and Robotics, Hunan University, China (email: kailun.yang@hnu.edu.cn).

<sup>2</sup>The authors are also with the Institute for Anthropomatics and Robotics, Karlsruhe Institute of Technology, Germany (email: kunyu.peng@kit.edu).

<sup>3</sup>The author is also with INSAIT, Sofia University “St. Kliment Ohridski”, Bulgaria.

<sup>4</sup>The author is also with the National Engineering Research Center of Robot Visual Perception and Control Technology, Hunan University, China.

\*Equal contribution.

†Corresponding authors: Kailun Yang and Kunyu Peng.

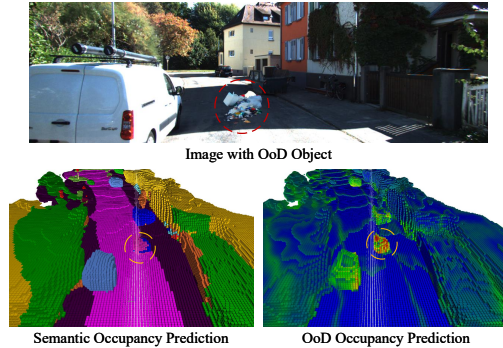


Fig. 1: Visualization of the established task of **Out-of-Distribution Semantic Occupancy Prediction**. The mainstream semantic occupancy prediction methods tend to misclassify Out-of-Distribution (OoD) objects as inliers, thus endangering the safety of autonomous driving. Proposed OccOoD accurately identifies OoD objects, with anomaly scores visualized from low (blue) to high (red).

effective in controlled settings, this approach [11] exposes systems to vulnerabilities from OoD objects and anomalies commonly encountered in real-world scenarios [12], [13], as seen in Fig. 1 where the standard semantic occupancy prediction method [14] produces misclassifications. OoD detection, the ability to identify entities that substantially deviate from the training data distribution, remains a critical yet underexplored challenge. Such anomalies include unexpected obstacles (e.g., discarded furniture, stray wildlife, construction equipment), unusual road conditions (e.g., potholes, debris, or oil spills), and atypical weather (e.g., sudden fog, heavy rain, or snowdrifts). As existing systems may misinterpret or fail to detect these deviations, they pose significant safety risks, potentially leading to failures and even catastrophic consequences in autonomous driving.

To bridge this critical gap, we introduce the task of Out-of-Distribution Semantic Occupancy Prediction, aiming to advance semantic scene understanding by integrating 3D occupancy prediction with OoD detection. However, the lack of datasets annotated for both semantic occupancy and OoD objects hinders robust model development. To address this, we propose a *Realistic Anomaly Augmentation* that injects diverse anomalies into existing datasets, preserving realistic spatial and occlusion patterns. This pipeline enables the creation of two novel datasets, VAA-KITTI and VAA-KITTI-360, comprising 26 distinct categories of anomalies, where anomaly annotations encompass a diverse range of unforeseen hazards, facilitating comprehensive evaluation of OoD detection in 3D scene understanding. To explore real-

world generalization, we further contribute VAA-STU, a real-world anomaly dataset for evaluation purposes.

Building upon our newly proposed datasets, we introduce OccOoD, the first unified framework that seamlessly unifies semantic occupancy prediction with OoD detection. First, we propose Cross-Space Semantic Refinement (CSSR), which refines semantic predictions by integrating complementary voxel and BEV features, where BEV provides enhanced global context to supplement local voxel representations, thereby improving both occupancy prediction robustness and OoD detection effectiveness. Second, we introduce an OoD detection mechanism leveraging entropy and cosine similarity, enabling effective identification of anomalies in dynamic, unstructured scenes. Furthermore, to ensure comprehensive and realistic evaluation, we conduct extensive OoD detection experiments on the newly proposed datasets and validate on the real-world VAA-STU dataset, while evaluating occupancy prediction on public benchmarks. Experimental results show that OccOoD achieves AuROC scores of 65.50% and 47.90% on the proposed datasets, 65.37% on VAA-STU, and mIoU scores of 16.80% and 18.37% on SemanticKITTI [15] and SSCBench-KITTI-360 [16], respectively. These results collectively establish OccOoD as a robust solution for addressing OoD challenges in 3D semantic occupancy prediction, demonstrating generalization to real-world environments.

In a nutshell, our contributions are threefold:

- We for the first time introduce out-of-distribution detection into the task of semantic occupancy prediction by delivering two new tailored datasets, VAA-KITTI and VAA-KITTI-360, specifically designed to evaluate OoD detection in the context of autonomous driving safety.
- We propose OccOoD, a unified framework that jointly handles 3D semantic occupancy prediction and OoD detection by fusing front-view and bird’s-eye-view representations, which provides the comprehensive spatial awareness required to robustly identify outliers.
- Our proposed framework, OccOoD, achieves state-of-the-art OoD detection performance on the established datasets while maintaining competitive accuracy in semantic occupancy prediction.

## II. RELATED WORK

**Semantic Occupancy Prediction.** 3D semantic occupancy prediction aims to infer both the geometry and semantics of a scene by inferring the occupancy state of voxels [17]. To advance estimation quality and efficiency, efforts are made in 3D representation [18], [19], context enhancement [20], [21], modality fusion [9], [22], and long-sequence and generative modeling [23], [24]. These efforts have collectively improved the quality and efficiency of semantic occupancy prediction. Recently, several works [5], [25] have introduced more fine-grained feature processing techniques. Meanwhile, uncertainty-aware methods [26], [27] incorporate uncertainty quantification to enhance estimation reliability. However, these methods are limited to predefined categories, requiring retraining to generalize to novel object types and lacking

flexibility. While open-vocabulary learning [28]–[31] addresses generalization to arbitrary categories, it remains constrained to In-Distribution (ID) scenarios and fails to handle OoD detection. In real-world applications, the categories of anomalous objects are unforeseeable, making such methods less reliable. In contrast, our proposed model extends semantic occupancy prediction by perceiving all OoD objects, enabling efficient and comprehensive scene understanding.

**Out-of-Distribution Segmentation.** Out-of-distribution segmentation identifies anomalies in specific scenes [12], [13] while maintaining in-distribution segmentation capabilities. Current research primarily focuses on anomaly detection in 2D images of road scenes, with the main methods including per-pixel architectures and mask-transformer-based approaches [32], [33]. The per-pixel architecture methods include uncertainty-based [34], [35], reconstruction-based [36], [37], and outlier exposure [38], [39] methods. While advancing 2D detection, these methods are constrained by pinhole camera inputs, which limits their applicability in 3D scenarios demanding precise spatial perception. Some studies extend anomaly detection to 3D space, yet primarily target industrial [40], [41] or indoor object inspection [42], [43], typically relying on static point clouds for defect localization [44], [45]. Due to their dependence on static geometric consistency and limited responsiveness to dynamic changes, these approaches are unsuitable for unconstrained, evolving environments. In contrast, we integrate out-of-distribution segmentation into vision-based 3D semantic occupancy prediction, enabling effective response to real-time changes and uncertainties, thereby overcoming the limitations of current methods in dynamic settings.

## III. OUT-OF-DISTRIBUTION DATASETS

To address the lack of evaluation platforms, we propose a *Realistic Anomaly Augmentation* to generate abnormal objects in real road scene images, leading to the creation of a suite of datasets: **VAA-KITTI**, **VAA-KITTI-360**, and **VAA-STU**. The former two are generated with realistic spatial and occlusion patterns, while VAA-STU is derived from a real-world 3D point cloud dataset [46] containing natural outliers, with scenes voxelized for occupancy prediction, enabling evaluation under real-world OoD conditions.

### A. Realistic Anomaly Augmentation

Collecting images and point cloud data of OoD objects is challenging due to their rarity in real-world scenes and the high cost of data collection and annotation. To address this, we propose a *Realistic Anomaly Augmentation* that generates synthetic anomalies under physical and environmental constraints, ensuring plausibility and challenge for robust OoD detection model evaluation. As illustrated in Fig. 2, our pipeline is structured into three key phases:

**Phase 1: Anomaly Generation and Localization.** In 2D anomaly detection, studies have demonstrated that synthetic anomaly data is highly effective for model training and evaluation [47], [48]. We employ POC [47], a state-of-the-art image generation technique, to synthesize anomaly images

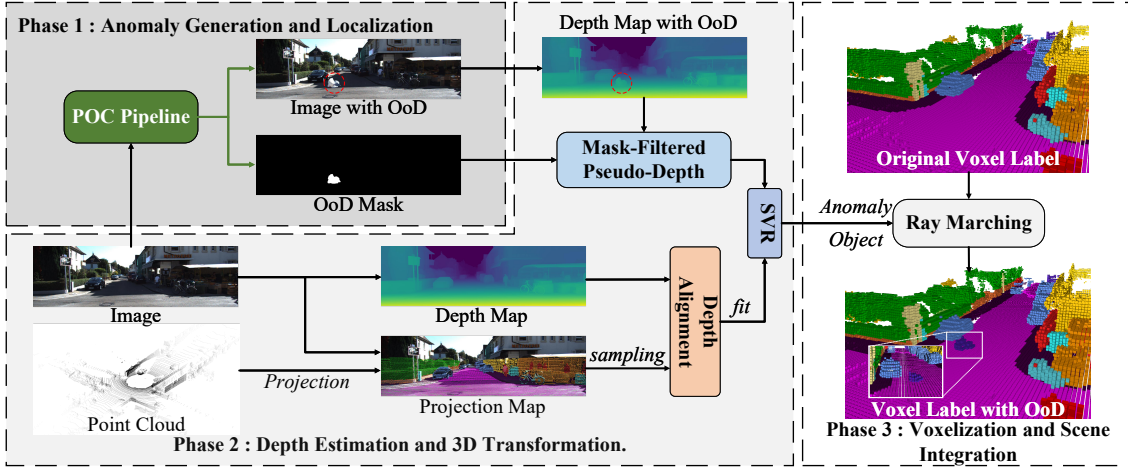


Fig. 2: An illustration of the proposed Realistic Anomaly Augmentation. This pipeline is designed to address the challenges of collecting real-world OoD data by synthesizing anomalies that are physically plausible and contextually realistic.

and their corresponding mask maps. To better align with real-world application scenarios, we introduce multi-category anomalies into the images, as illustrated in Fig. 3.

### Phase 2: Depth Estimation and 3D Transformation.

This phase integrates images with accurate depth to enable transformation of 2D anomaly detections into precise 3D spatial localization. To address limited metric depth accuracy, we project synthesized anomalies into the 3D point cloud.

Specifically, we first utilize the large version of Depth Anything V2 [49], to compute pseudo-depth for both original and synthesized images. Subsequently, we randomly sample a predefined number of points, from the point cloud and project them onto the image plane to obtain pixel coordinates  $\mathbf{u}_i$  and Euclidean distances  $d_i$  as:

$$\mathbf{u}_i = \frac{\mathbf{K} \cdot (\mathbf{R}\mathbf{p}_i + \mathbf{t})}{[\mathbf{R}\mathbf{p}_i + \mathbf{t}]_z}, \quad (1)$$

$$d_i = \|\mathbf{R}\mathbf{p}_i + \mathbf{t}\|_2,$$

where  $\mathbf{p}_i$  is a 3D point,  $\mathbf{K}$  is the camera intrinsic matrix,  $\mathbf{R}$  and  $\mathbf{t}$  are the rotation and translation of the camera,  $\mathbf{u}_i$  is the projected 2D point, and  $d_i$  is the Euclidean distance.

By utilizing  $\mathbf{u}_i$  and the previously obtained depth map, we align the pseudo-depth with the real depth and apply Support Vector Regression (SVR) [50] for nonlinear regression, mapping the pseudo-depth to real-world depth. Finally, the aligned depth map and mask map from Phase 1 are used to derive 3D anomaly coordinates  $(u, v, d)$ , which are then transformed into the 3D voxel space.

**Phase 3: Voxelization and Scene Integration.** The pseudo-point clouds of anomalies are voxelized and integrated into the 3D voxel space of the original point cloud. Leveraging camera poses, we project each anomaly point  $\mathbf{A}_i^v = (x_i^v, y_i^v, z_i^v)$  (representing the discrete voxel coordinates of the  $i$ -th anomaly) back into the scene to determine occlusion relationships via ray marching. The ray position of the ray at step  $k$  is computed as:

$$\mathbf{c}_k = \mathbf{C}^v + k \cdot \frac{\mathbf{A}_i^v - \mathbf{C}^v}{\|\mathbf{A}_i^v - \mathbf{C}^v\|_2}, \quad (2)$$

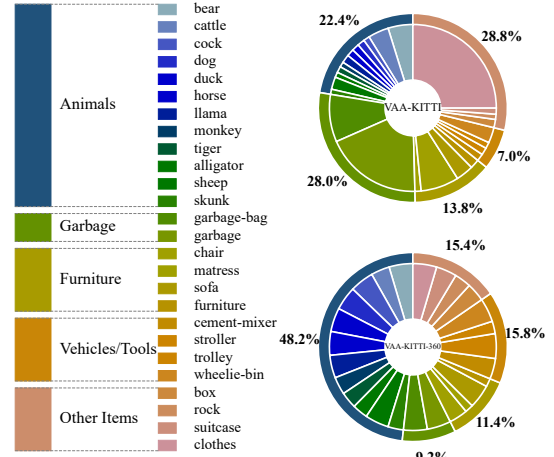


Fig. 3: Distribution map of VAA-KITTI and VAA-KITTI-360, containing 26 distinct OoD categories grouped into five main types as shown.

where  $k$  is the step index,  $\mathbf{c}_k$  is the ray position at  $k$ ,  $\mathbf{C}^v$  is the camera position and  $\mathbf{v}_k = \text{round}(\mathbf{c}_k)$  is the corresponding voxel center. The step size is controlled by a scaling factor  $s > 0$ , with  $\Delta = \frac{1}{s}$  defining the resolution.

The occlusion process is formalized as:

$$\mathbf{V}[\mathbf{v}_k] = \begin{cases} 1, & \text{if } \|\mathbf{c}_k - \mathbf{A}_i^v\|_2 \leq \Delta, \\ 0, & \text{otherwise.} \end{cases} \quad (3)$$

where 0 and 1 represent the occupancy status of the voxel.

### B. VAA-KITTI, VAA-KITTI-360, and VAA-STU

We applied the aforementioned synthesis pipeline to SemanticKITTI [15] and SSCBench-KITTI-360 [16], creating two fresh datasets: VAA-KITTI and VAA-KITTI-360. These datasets extend the original labels with outliers, encompassing 26 distinct anomaly categories.

To ensure the plausibility and naturalness, over 30,000 images produced using the POC algorithm were carefully reviewed by three independent annotators. After multiple

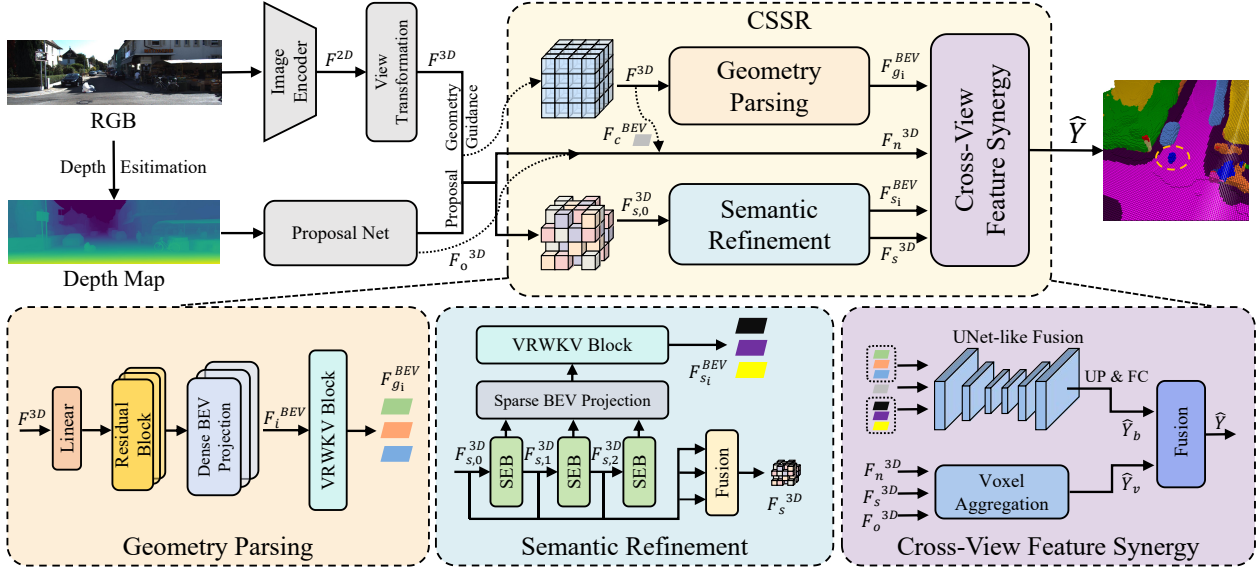


Fig. 4: An overview of the proposed OccOoD framework. The image encoder extracts 2D features and converts them into 3D features via View Transformation, guided by geometric occupancy. Seed voxels and other features are processed through Geometry Pairing and Semantic Refinement to generate enhanced BEV and voxel features. Finally, Cross-View Feature Synergy integrates these representations for rich geometry and high spatial efficiency.

rounds of cross-checking, images with poor generation quality, implausible object placements, or non-anomalous scenarios (e.g., *birds flying in an urban sky or trash and wheeled bins placed alongside sidewalks*) are excluded, yielding a final selection of 500 images for both the VAA-KITTI and VAA-KITTI-360 test sets in the Out-of-Distribution Semantic Occupancy Prediction task.

In addition, we construct VAA-STU from a real-world 3D LiDAR dataset featuring real anomalous objects with precise instance annotations. It includes two sequences from STU [46], voxelized into a format compatible with occupancy models, preserving real-world environmental complexity for the robust OoD evaluation.

**Regional-Level Metrics Design.** Referring to 2D image anomaly detection [33], we adopt Area under the Receiver Operating Characteristic Curve (AuROC) as a performance metric. Furthermore, to mitigate the evaluation impact caused by the inaccuracy of existing methods in predicting the absolute positions of instances, and bridge the gap between localization demands and anomaly-awareness goals, we propose a regional-level metric: Regional Area under the Precision-Recall Curve (AuPRC<sub>r</sub>). The AuPRC<sub>r</sub> incorporates tolerance for minor localization inaccuracies while maintaining sensitivity to anomaly detection.

**AuPRC<sub>r</sub>:** The Precision-Recall curve evaluates the balance between precision and recall at varying thresholds:

$$\text{Precision}_r = \frac{\text{TP}_r}{\text{TP}_r + \text{FP}_r}, \quad \text{Recall}_r = \frac{\text{TP}_r}{\text{TP}_r + \text{FN}_r}, \quad (4)$$

where  $\text{TP}_r$ ,  $\text{FP}_r$ , and  $\text{FN}_r$  denote true positives, false positives, and false negatives within a regional tolerance radius  $r$ . The AuPRC<sub>r</sub> is computed as Eq. (5):

$$\text{AuPRC}_r = \int_0^1 \text{Precision}_r(\text{Recall}_r) d(\text{Recall}_r). \quad (5)$$

## IV. OCCOOD: PROPOSED FRAMEWORK

### A. Problem Setting

Out-of-distribution segmentation in 2D pinhole images typically relies on pixel-wise anomaly scores. Building on this concept, we extend out-of-distribution detection to 3D semantic occupancy prediction at the voxel level. Given an input image, the semantic occupancy prediction process yields a volumetric representation  $V \in \mathbb{R}^{C \times H \times W \times Z}$ , where  $C$ ,  $H$ ,  $W$ , and  $Z$  correspond to the channels, height, width, and depth of the voxel space, respectively. The voxel-level classification scores  $Q(V) \in \mathbb{R}^{K \times H \times W \times Z}$  are then obtained, and  $K$  denotes the number of classes for the semantic prediction. Ultimately, to assess anomalies at the voxel level, an anomaly score  $A(V) \in \mathbb{R}^{H \times W \times Z}$  is computed as Eq. (6):

$$A(V) = f(Q(V)). \quad (6)$$

### B. Overall Architecture

The OccOoD framework, illustrated in Fig. 4, integrates front-view and BEV representations for precise 3D semantic occupancy prediction. 3D voxels preserve fine geometric details, while BEV enhances spatial reasoning and global understanding. To leverage their complementary strengths, we propose the Cross-Space Semantic Refinement (CSSR), which extracts and refines features across both spaces. By fusing multi-scale representations across spaces, CSSR enhances feature representation, sharpens boundaries, and improves OoD detection. Following SGN [14], 2D features extracted from RGB images are transformed into 3D voxel representations via a view transformation module based on MonoScene [2]. These coarse features are refined through a geometry-guided auxiliary 3D occupancy head, supervised by a binary cross-entropy loss  $L_{\text{geo}}$ , and subsequently filtered by a proposal network trained with an additional binary

cross-entropy loss  $L_{occ}$ . The filtered features then undergo Geometry Parsing and Semantic Refinement to extract multi-scale BEV features encoding spatial structure and fine-grained semantic voxel features. These BEV features are fused with the original 3D features through a UNet-like module, ensuring precise alignment and enhanced learning. Finally, the upsampled BEV representation is combined with the aggregated voxel features through a 1D convolutional layer to produce the final semantic occupancy prediction.

### C. Cross-Space Semantic Refinement

The coarse voxel features  $F^{3D}$  from the view transformation module and the seed features  $F_{s,0}^{3D}$  from the proposal network are in 3D voxel space. However, relying solely on voxel features limits semantic detail and boundary clarity, harming OoD detection. To address this, we propose Cross-Space Semantic Refinement (CSSR), which leverages voxel and BEV representations to enhance semantic prediction. Features are refined separately in the BEV space to capture global contextual structure and in the voxel space to preserve fine-grained local details and fused to produce accurate occupancy predictions with improved OoD sensitivity.

**Geometry Parsing.** As shown in Fig. 4, the coarse voxel features  $F^{3D}$  are processed through a geometric parsing branch to extract compact BEV representations encoding spatial structure. This branch projects  $F^{3D}$  into a lower-dimensional space, applies residual refinement and z-axis alignment, then compresses it via 2D convolutions to generate dense BEV features. These are enhanced by the Vision-RWKV (VRWKV) module [51] through spatial and channel mixing, yielding dense geometric BEV features  $\{F_{g_i}^{BEV}\}_i$ .

**Semantic Refinement.** The seed voxels  $F_{s,0}^{3D}$  from the proposal network undergo semantic refinement to enhance accuracy. The module comprises three cascaded sparse encoder blocks (SEBs), each linked with a BEV projection and a VRWKV block. Each SEB contains a Sparse Feature Encoder (SFE) [52] and a Sparse Geometry Feature Encoder (SGFE) [52], which refine the initial representation through hierarchical pooling and attention, capturing fine-grained details and contextual dependencies.

First, the multi-scale features  $F_{s,1}^{3D}$  and  $F_{s,2}^{3D}$  output by the first two SEBs are projected into BEV space via max-pooling, generating sparse features. These are densified using Spconv and enhanced by the VRWKV module [51] to model long-range dependencies, yielding multi-scale semantic BEV features  $\{F_{s_i}^{BEV}\}_i$ . The refined voxel features  $F_s^{3D}$  are obtained by fusing  $F_{s,0}^{3D}$ ,  $F_{s,1}^{3D}$ , and  $F_{s,2}^{3D}$  via an MLP (Eq. 7):

$$F_s^{3D} = \text{MLP}([F_{s,0}^{3D}, F_{s,1}^{3D}, F_{s,2}^{3D}]). \quad (7)$$

The multi-scale semantic BEV features  $\{F_{s_i}^{BEV}\}_i$  are used for BEV-level fusion, while the refined semantic feature  $F_s^{3D}$  is utilized for voxel-level fusion. Additionally,  $F_s^{3D}$  is passed through an auxiliary semantic head (a two-layer MLP) to predict the corresponding semantics  $\hat{Y}_s$ .

The semantic refinement stage is optimized using a combined loss of cross-entropy and Lovasz loss [53] as follows:

$$L_{sem} = L_{ce}(\hat{Y}_s, Y_s) + L_{lovasz}(\hat{Y}_s, Y_s), \quad (8)$$

where  $Y_s$  represents the semantic labels of seed voxels.

**Cross-View Feature Synergy.** To integrate BEV and voxel-level representations, we process them in parallel.

For the BEV branch, a UNet-like architecture encodes hierarchical spatial features and decodes high-resolution maps for fusion, including the projected 3D features  $F_c^{BEV}$ , geometric BEV features  $\{F_{g_i}^{BEV}\}_i$ , and semantic BEV features  $\{F_{s_i}^{BEV}\}_i$ . The encoder downsamples  $F_c^{BEV}$  through convolutional blocks, each followed by a VRWKV block, and fuses the three BEV streams using an ARF module [54]:

$$F_f^{BEV} = \sum_{k \in \{g, s, c\}} (F_{k_i}^{BEV} \odot A_{k_i}^{BEV}), \quad (9)$$

where  $F_{k_i}^{BEV}$  and  $A_{k_i}^{BEV}$  denote the  $k$ -th feature map and its attention weight, respectively. The decoder restores resolution via transposed convolutions and skip connections, and the output is reshaped and upsampled to yield a voxel-level representation  $\hat{Y}_b$ .

For the voxel branch, we follow SGN [14], fusing refined semantic features  $F_s^{3D}$ , non-seed features  $F_n^{3D}$ , and occupancy features  $F_o^{3D}$  via Multi-Scale Semantic Propagation (MSSP) as follows:

$$\hat{Y}_v = \text{MSSP}([F_s^{3D}, F_n^{3D}, F_o^{3D}]). \quad (10)$$

Subsequently,  $\hat{Y}_v$  and  $\hat{Y}_b$  are fused via a 1D convolutional layer to produce the final prediction  $\hat{Y}_f$ . The model is optimized with a combined loss as follows:

$$L_{ssc} = L_{sem}^{scal}(\hat{Y}, Y) + L_{geo}^{scal}(\hat{Y}, Y) + L_{ce}(\hat{Y}, Y), \quad (11)$$

where  $L_{sem}^{scal}$  ensures semantic consistency at both scene and class levels,  $L_{geo}^{scal}$  enforces geometric fidelity, and  $L_{ce}$  minimizes classification errors.

**Loss Function.** The total training loss is defined as follows:

$$L = L_{geo} + L_{occ} + L_{sem} + L_{ssc}. \quad (12)$$

### D. OoD Occupancy Prediction

After achieving high-precision semantic occupancy prediction, we further integrate an out-of-distribution detection mechanism to identify outliers that deviate from the in-distribution regions. For the semantic occupancy prediction results  $\hat{Y}_f$ , we compute the category-specific anomaly score  $A(V)$  for each voxel according to the predictive semantics.

**Geometry Prior.** To more efficiently focus on non-empty regions, we introduce a geometry prior by applying an *argmax* operation to  $\hat{Y}_f$ . This strategy prioritizes potentially anomalous non-empty regions, significantly improving the effectiveness and accuracy of OoD detection.

**Anomalis-Sensitive Scoring.** We compute anomaly scores based on the predicted semantic category, employing distinct strategies to capture the two primary forms of uncertainty pertinent to OoD detection.

- For **instance** (e.g., *car*, *person*), which form compact clusters in the logit space, anomalies appear as outliers from the class centroid. We measure this deviation using *cosine similarity*:

$$S_{\text{cosine}}(v_i) = 1 - \cos(\mathbf{1}(v_i), \bar{\mathbf{1}}), \quad (13)$$

TABLE I: Quantitative results on the SemanticKITTI validation set [15] and VAA-KITTI. The best and the second best results are in **bold** and under lined, respectively.

Method	IoU	road	sidewalk	parking	otherground	building	car	truck	bicycle	motorcycle	othervehicle	vegetation	trunk	terrain	person	bicyclist	motorcyclist	fence	pole	trafficsign	mIoU
		■	■	■	■	■	■	■	■	■	■	■	■	■	■	■	■	■	■	■	
SemanticKITTI																					
MonoScene [2]	37.12	57.47	27.05	15.72	<b>0.87</b>	14.24	23.55	7.83	0.20	0.77	3.59	18.12	2.57	30.76	<u>1.79</u>	<u>1.03</u>	0.00	6.39	4.11	2.48	11.50
SGN [14]	<u>46.21</u>	59.10	29.41	19.05	<u>0.33</u>	<u>25.17</u>	33.31	6.03	0.61	0.46	<u>9.84</u>	<b>28.93</b>	<b>9.58</b>	<u>38.12</u>	0.47	0.10	0.00	<b>9.96</b>	<b>13.25</b>	<u>7.21</u>	15.32
CGFormer [5]	45.99	<b>65.51</b>	<b>32.31</b>	<u>20.82</u>	0.16	23.52	<b>34.32</b>	<u>19.44</u>	<b>4.61</b>	<b>2.71</b>	7.67	26.93	8.83	<b>39.54</b>	<b>2.38</b>	<b>4.08</b>	0.00	9.20	10.67	<b>7.84</b>	<b>16.89</b>
OccOoD (Ours)	<b>46.83</b>	<u>60.87</u>	<u>32.16</u>	<b>23.52</b>	0.06	<b>26.54</b>	<u>33.51</u>	<b>25.17</b>	<u>0.65</u>	<u>1.00</u>	<b>11.84</b>	<u>28.43</u>	<u>8.90</u>	36.96	0.44	0.16	0.00	<u>9.94</u>	<u>13.00</u>	6.03	<u>16.80</u>
VAA-KITTI																					
SGN [14]	<u>39.07</u>	<u>46.62</u>	<u>26.54</u>	15.88	<b>0.12</b>	<b>18.34</b>	<b>20.51</b>	<u>0.62</u>	<b>0.44</b>	<u>0.35</u>	<b>1.23</b>	24.76	<b>6.40</b>	21.78	0.48	1.29	0.00	<b>12.25</b>	<b>8.70</b>	<u>4.57</u>	<u>11.10</u>
OccOoD (Ours)	<b>40.04</b>	<b>50.17</b>	<b>27.42</b>	<b>18.40</b>	<u>0.01</u>	<u>17.38</u>	<u>20.19</u>	<b>0.74</b>	<u>0.26</u>	<b>0.56</b>	<u>1.04</u>	<b>25.13</b>	<u>5.53</u>	<b>23.56</b>	<b>0.67</b>	<b>1.95</b>	0.00	<u>11.35</u>	<u>8.15</u>	<b>5.80</b>	<b>11.49</b>

TABLE II: OoD detection performance on VAA-KITTI dataset. Best results in **bold**.

Methods	VAA-KITTI			AuROC $\uparrow$
	AuPRC $_r\uparrow$			
	0.8m	1.0m	1.2m	
Monoscene [2]	2.81	3.48	4.31	63.54
CGFormer [5]	5.65	6.44	7.36	64.09
SGN [14]	12.69	18.81	27.10	65.40
OccOoD (ours)	<b>17.15</b>	<b>23.48</b>	<b>31.83</b>	<b>65.50</b>

where  $\mathbf{l}(v_i)$  is the logit vector of voxel  $v_i$ , and  $\bar{\mathbf{l}}$  is the mean logit vector of the same class.

- For **region** (e.g., road, vegetation), which occupy large, homogeneous areas, OoD regions typically induce high prediction uncertainty. This is quantified using *entropy*:

$$S_{\text{entropy}}(v_i) = - \sum_{k \in \mathcal{K}} p(k|v_i) \log p(k|v_i), \quad (14)$$

where  $\mathcal{K}$  represents the set of possible classes, and  $p(k|v_i)$  is the predicted probability of class  $k$  for voxel  $v_i$ . To prioritize detection around structured instance classes, the entropy-based scores for region classes are down-weighted. Higher entropy indicates greater uncertainty, a hallmark of OoD regions.

Ultimately, the anomaly scores  $A(V)$  are normalized to  $[0, 1]$  to ensure comparability across classes. Voxels predicted as empty are assigned the minimum anomaly score, effectively filtering them from further analysis.

## V. EXPERIMENTS

### A. Implementation Details

We train OccOoD (38M parameters) for 35 epochs on 4 RTX3090 GPUs with a batch size of 4, using AdamW with a learning rate of  $2e-4$  and weight decay of  $1e-2$ . We evaluate OccOoD’s semantic occupancy prediction on public benchmarks. For OoD detection, our evaluation is conducted on the proposed datasets with single-frame settings.

TABLE III: OoD detection performance on VAA-KITTI-360 and VAA-STU datasets. Best results in **bold**.

Methods	VAA-KITTI-360				VAA-STU			
	0.8m	AuPRC $_r\uparrow$ 1.0m	1.2m	AuROC $\uparrow$	0.8m	AuPRC $_r\uparrow$ 1.0m	1.2m	AuROC $\uparrow$
SGN [14]	12.24	24.89	45.15	45.06	2.91	5.74	11.32	64.51
OccOoD (ours)	<b>12.84</b>	<b>25.74</b>	<b>46.28</b>	<b>47.90</b>	<b>3.05</b>	<b>6.15</b>	<b>11.39</b>	<b>65.37</b>

### B. Quantitative Results

**Out-of-Distribution Detection.** In Table II and III, the OoD detection results are reported. Across the three scales of AuPRC $_r$ , our network achieves a significant improvement over the baseline. On the VAA-KITTI dataset, our performance improves by more than 4% in terms of AuPRC $_r$ . Similarly, on both the VAA-KITTI-360 and VAA-STU datasets, our method demonstrates superior performance. Notably, CGFormer [5] underperforms in OoD detection despite strong in-distribution accuracy. When encountering anomalies (e.g., animals, garbage bags), it often assigns them to rare in-distribution categories such as *bicycle* and *motorcycle* with high confidence, lacking clear semantic correspondence. This overconfident misclassification reflects poor model calibration and an inability to recognize distributional novelty. By enforcing consistency between voxel and BEV spaces, CSSR reduces overconfident misclassification and enhances sensitivity to anomalies.

**3D Occupancy Prediction.** We present the experimental results of semantic occupancy prediction in Table I and Table IV. Our method consistently demonstrates performance improvements over the baseline model, regardless of whether the evaluation is conducted on public datasets or our self-constructed datasets. These results validate the effectiveness of our designed CSSR, which leverages complementary strengths of voxel and BEV representations to enhance semantic refinement and global context modeling.

### C. Ablation Studies

**Anomalis-Sensitive Scoring.** Table V demonstrates the effectiveness of our proposed Anomalis-Sensitive Scoring (ASS). Compared to the other three scoring methods, our

TABLE IV: Quantitative results on the SSCBench-KITTI360 test set [16] and VAA-KITTI-360. The results for counterparts are provided in [16]. The best and the second best results are in **bold** and under lined, respectively.

Method	IoU	car	bicycle	motorcycle	truck	other-veh.	person	road	parking	sidewalk	other-grnd.	building	fence	vegetation	terrain	pole	traf.sign	other-struct.	other-obj.	mIoU
		■	■	■	■	■	■	■	■	■	■	■	■	■	■	■	■	■	■	
SSCBench-KITTI-360																				
MonoScene [2]	37.87	19.34	0.43	0.58	8.02	2.03	0.86	48.35	11.38	28.13	3.32	32.89	3.53	26.15	16.75	6.92	5.67	4.20	3.09	12.31
VoxFormer [4]	38.76	17.84	1.16	0.89	4.56	2.06	1.63	47.01	9.67	27.21	2.89	31.18	4.97	28.99	14.69	6.51	6.92	3.79	2.43	11.91
SGN [14]	47.06	<u>29.03</u>	<b>3.43</b>	<u>2.90</u>	<u>10.89</u>	<u>5.20</u>	2.99	58.14	15.04	36.40	4.43	42.02	7.72	<u>38.17</u>	<u>23.22</u>	<u>16.73</u>	16.38	<u>9.93</u>	5.86	18.25
CGFormer [5]	<b>48.07</b>	<u>29.85</u>	<u>3.42</u>	<b>3.96</b>	<u>17.59</u>	<b>6.79</b>	<b>6.63</b>	<b>63.85</b>	<b>17.15</b>	<b>40.72</b>	<b>5.53</b>	<u>42.73</u>	<b>8.22</b>	<b>38.80</b>	<b>24.94</b>	16.24	<u>17.45</u>	<b>10.18</b>	<u>6.77</u>	<b>20.05</b>
OccOoD (Ours)	46.93	28.51	2.95	0.94	9.48	4.57	<u>2.99</u>	<u>58.91</u>	<u>16.17</u>	<u>37.04</u>	5.34	<b>42.99</b>	<u>7.83</u>	37.41	23.01	<b>17.47</b>	<b>18.87</b>	8.94	<b>7.16</b>	<u>18.37</u>
VAA-KITTI-360																				
SGN [14]	<b>39.90</b>	<u>21.93</u>	<b>0.04</b>	0.00	0.00	<u>0.66</u>	<b>0.88</b>	46.95	<u>13.81</u>	<u>25.67</u>	<u>2.72</u>	<b>33.31</b>	<b>3.07</b>	<b>28.25</b>	<b>12.63</b>	<b>8.95</b>	<b>13.84</b>	<b>3.79</b>	<u>1.52</u>	<u>12.11</u>
OccOoD (Ours)	39.26	<b>22.84</b>	<u>0.00</u>	0.00	0.00	<b>3.54</b>	<u>0.58</u>	<b>49.09</b>	<b>14.65</b>	<b>27.84</b>	<b>3.41</b>	<u>32.59</u>	1.55	<u>27.46</u>	<u>11.46</u>	8.42	<u>12.30</u>	3.63	<b>6.49</b>	<b>12.55</b>

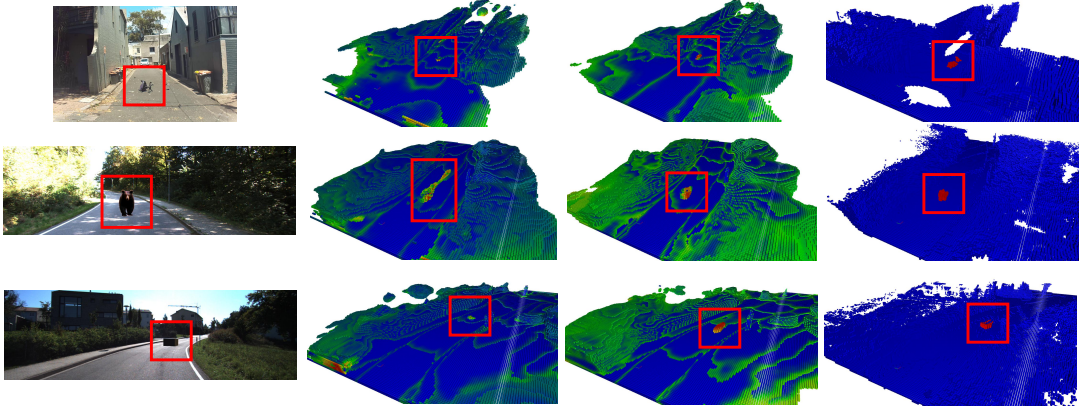


Fig. 5: Visualization of the results on VAA-KITTI and VAA-STU datasets. From left to right are the input RGB images, the SGN [14] results, the OccOoD (ours) results, and the OoD ground truths. **Zoom in for a better view.**

TABLE V: Ablation studies of ASS on VAA-KITTI.

Anomaly Score Methods	VAA-KITTI			
	0.8m	1.0m	1.2m	AuROC $\uparrow$
Entropy	7.11	12.26	19.95	65.19
Postpro	5.83	9.92	15.94	64.88
Energy	7.24	12.40	20.05	64.78
ASS (Ours)	<b>17.15</b>	<b>23.48</b>	<b>31.83</b>	<b>65.50</b>

approach improves  $AuPRC_r$  by more than 10% across all scales. This improvement stems from our dual-strategy design, which applies cosine similarity to compact instances and entropy to homogeneous regions, effectively matching the scoring to each object’s spatial characteristics for better OoD identification.

**Geometry Prior.** Table VI evaluates the role of the geometry prior via  $AuPRC_r$  and AuROC. Including the prior substantially improves  $AuPRC_r$ . Without it, the higher AuROC arises because empty voxel uncertainty is also scored as anomalous. Given the scarcity of positive samples in our dataset,  $AuPRC_r$  is the more appropriate performance metric.

#### D. Qualitative Results

**Qualitative Comparison.** As shown in Fig. 5, unlike SGN [14] which solely relies on voxel input and produces

TABLE VI: Ablation studies of geometry prior within 1.2m.

Methods	VAA-KITTI		VAA-KITTI-360	
	$AuPRC_r\uparrow$	AuROC $\uparrow$	$AuPRC_r\uparrow$	AuROC $\uparrow$
w/o Geometry prior	14.86	<b>76.59</b>	35.17	36.72
Geometry prior	<b>31.83</b>	65.50	<b>46.28</b>	<b>47.90</b>

inconsistent shape estimations, our method leverages the complementary strengths of voxel and BEV features through CSSR, effectively improving the localization of small objects (e.g., *chair*) and maintaining the structural continuity of larger ones (e.g., *bear*), leading to more complete and geometrically coherent occupancy estimates, ultimately leading to improved OoD detection performance.

**Insights Into Real-World Applications.** Fig. 6 presents results from a real-world urban environment beyond the VAA-STU dataset. We collected additional real urban scenes using a ZED Mini camera and ran inference on the captured left-view images. The model demonstrates practical efficiency, achieving 9 FPS on a consumer-grade GPU RTX3090. The left image contains an OoD object (a box on the road). The 3D occupancy prediction (middle) misclassifies it as a motorcycle, exposing a key limitation. In contrast, our pro-

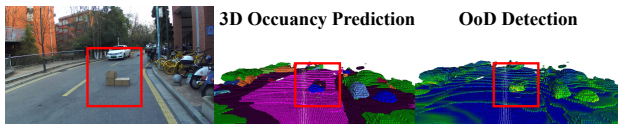


Fig. 6: Results in real-world urban environments.

posed OoD detection (right) correctly identifies this anomaly with high confidence, demonstrating the method’s ability to generalize to unseen scenarios and its potential to enhance the safety and reliability of autonomous driving systems.

## VI. CONCLUSION

In this paper, we look into out-of-distribution semantic occupancy prediction to address OoD voxel detection in 3D space. To address the lack of anomaly annotations in existing datasets, we propose a Realistic Anomaly Augmentation and develop three evaluation datasets: VAA-KITTI, VAA-KITTI-360, and VAA-STU. Our method, OccOoD, integrates OoD detection into 3D semantic occupancy prediction by combining voxel-based and BEV representations, effectively capturing both local detail and global context for enhanced semantic and geometric reasoning. Experiments show that OccOoD achieves state-of-the-art OoD detection performance on these datasets while maintaining competitive occupancy prediction accuracy on standard benchmarks.

## REFERENCES

- [1] Y. Hu *et al.*, “Planning-oriented autonomous driving,” in *CVPR*, 2023.
- [2] A.-Q. Cao and R. De Charette, “MonoScene: Monocular 3D semantic scene completion,” in *CVPR*, 2022.
- [3] Y. Zhang, Z. Zhu, and D. Du, “OccFormer: Dual-path transformer for vision-based 3D semantic occupancy prediction,” in *ICCV*, 2023.
- [4] Y. Li *et al.*, “VoxFormer: Sparse voxel transformer for camera-based 3D semantic scene completion,” in *CVPR*, 2023.
- [5] Z. Yu *et al.*, “Context and geometry aware voxel transformer for semantic scene completion,” in *NeurIPS*, 2024.
- [6] R. Marcuzzi *et al.*, “SfmOcc: Vision-based 3D semantic occupancy prediction in urban environments,” *IEEE Robotics and Automation Letters*, 2025.
- [7] Q. Lai, H. Zheng, X. Feng, M. Zheng, H. Chen, and W. Chen, “RTONet: Real-time occupancy network for semantic scene completion,” *IEEE Robotics and Automation Letters*, 2024.
- [8] J. Pan, Z. Wang, and L. Wang, “Co-Occ: Coupling explicit feature fusion with volume rendering regularization for multi-modal 3D semantic occupancy prediction,” *IEEE Robotics and Automation Letters*, 2024.
- [9] Y. Ma *et al.*, “LiCROcc: Teach radar for accurate semantic occupancy prediction using LiDAR and camera,” *IEEE Robotics and Automation Letters*, 2025.
- [10] Z. Liu *et al.*, “Sparse annotation, dense supervision: Unleashing self-training power for occupancy prediction with 2D labels,” *IEEE Robotics and Automation Letters*, 2026.
- [11] Z. Li *et al.*, “BEVFormer: Learning bird’s-eye-view representation from multi-camera images via spatiotemporal transformers,” in *ECCV*, 2022.
- [12] H. Blum, P.-E. Sarlin, J. Nieto, R. Siegwart, and C. Cadena, “The fishyscapes benchmark: Measuring blind spots in semantic segmentation,” *International Journal of Computer Vision*, 2021.
- [13] R. Chan *et al.*, “SegmentMeIfYouCan: A benchmark for anomaly segmentation,” in *NeurIPS*, 2021.
- [14] J. Mei *et al.*, “Camera-based 3D semantic scene completion with sparse guidance network,” *IEEE Transactions on Image Processing*, 2024.
- [15] J. Behley *et al.*, “SemanticKITTI: A dataset for semantic scene understanding of LiDAR sequences,” in *ICCV*, 2019.
- [16] Y. Li *et al.*, “SSCBench: A large-scale 3D semantic scene completion benchmark for autonomous driving,” in *IROS*, 2024.
- [17] S. Song, F. Yu, A. Zeng, A. X. Chang, M. Savva, and T. Funkhouser, “Semantic scene completion from a single depth image,” in *CVPR*, 2017.
- [18] H. Liu *et al.*, “Fully sparse 3D occupancy prediction,” in *ECCV*, 2024.
- [19] Y. Lu, X. Zhu, T. Wang, and Y. Ma, “OctreeOcc: Efficient and multi-granularity occupancy prediction using octree queries,” in *NeurIPS*, 2024.
- [20] Y. Wang and C. Tong, “H2GFormer: Horizontal-to-global voxel transformer for 3D semantic scene completion,” in *AAAI*, 2024.
- [21] J. Li, X. He, C. Zhou, X. Cheng, Y. Wen, and D. Zhang, “ViewFormer: Exploring spatiotemporal modeling for multi-view 3D occupancy perception via view-guided transformers,” in *ECCV*, 2024.
- [22] H. Zhang *et al.*, “RadOcc: Learning cross-modality occupancy knowledge through rendering assisted distillation,” in *AAAI*, 2024.
- [23] J. Wang *et al.*, “OccRWKV: Rethinking efficient 3D semantic occupancy prediction with linear complexity,” in *ICRA*, 2025.
- [24] H. Li, Y. Hou, X. Xing, X. Sun, and Y. Zhang, “OccMamba: Semantic occupancy prediction with state space models,” in *CVPR*, 2025.
- [25] H. Jiang *et al.*, “Symphonize 3D semantic scene completion with contextual instance queries,” in *CVPR*, 2024.
- [26] J. Kälble, S. Wirges, M. Tatarchenko, and E. Ilg, “EvOcc: Accurate semantic occupancy for automated driving using evidence theory,” in *CVPR*, 2025.
- [27] S. Heidrich, T. Beemelmans, A. Nekrasov, B. Leibe, and L. Eckstein, “OCCUQ: Exploring efficient uncertainty quantification for 3D occupancy prediction,” in *ICRA*, 2025.
- [28] Z. Tan, Z. Dong, C. Zhang, W. Zhang, H. Ji, and H. Li, “OVO: Open-vocabulary occupancy,” *arXiv preprint arXiv:2305.16133*, 2023.
- [29] S. Boeder, F. Gigengack, and B. Risse, “LangOcc: Self-supervised open vocabulary occupancy estimation via volume rendering,” *arXiv preprint arXiv:2407.17310*, 2024.
- [30] A. Vobecky *et al.*, “POP-3D: Open-vocabulary 3D occupancy prediction from images,” in *NeurIPS*, 2024.
- [31] Z. Zhang, B. Gao, J. Ye, H. Jin, L. Jiang, and W. Yang, “CLIP prior-guided 3D open-vocabulary occupancy prediction,” *Pattern Recognition*, 2025.
- [32] S. N. Rai, F. Cermelli, B. Caputo, and C. Masone, “Mask2Anomaly: Mask transformer for universal open-set segmentation,” *IEEE Transactions on Pattern Analysis and Machine Intelligence*, 2024.
- [33] N. Nayal, M. Yavuz, J. F. Henriques, and F. Güney, “RbA: Segmenting unknown regions rejected by all,” in *ICCV*, 2023.
- [34] C. Corbière, N. Thome, A. Bar-Hen, M. Cord, and P. Pérez, “Addressing failure prediction by learning model confidence,” in *NeurIPS*, 2019.
- [35] S. Jung, J. Lee, D. Gwak, S. Choi, and J. Choo, “Standardized max logits: A simple yet effective approach for identifying unexpected road obstacles in urban-scene segmentation,” in *ICCV*, 2021.
- [36] K. Lis, K. Nakka, P. Fua, and M. Salzmann, “Detecting the unexpected via image resynthesis,” in *ICCV*, 2019.
- [37] M. Grcic, P. Bevanđic, Z. Kalafatic, and S. Segvic, “Dense anomaly detection by robust learning on synthetic negative data,” *arXiv preprint arXiv:2112.12833*, 2021.
- [38] Y. Tian, Y. Liu, G. Pang, F. Liu, Y. Chen, and G. Carneiro, “Pixel-wise energy-biased abstention learning for anomaly segmentation on complex urban driving scenes,” in *ECCV*, 2022.
- [39] M. Grcic, P. Bevanđic, and S. Segvic, “DenseHybrid: Hybrid anomaly detection for dense open-set recognition,” in *ECCV*, 2022.
- [40] P. Bergmann, X. Jin, D. Sattlegger, and C. Steger, “The MVTEC 3D-AD dataset for unsupervised 3D anomaly detection and localization,” in *VISAPP*, 2022.
- [41] J. Liu *et al.*, “Real3D-AD: A dataset of point cloud anomaly detection,” in *NeurIPS*, 2023.
- [42] A. Bhunia, C. Li, and H. Bilen, “Looking 3D: Anomaly detection with 2D-3D alignment,” in *CVPR*, 2024.
- [43] W. Li, X. Xu, Y. Gu, B. Zheng, S. Gao, and Y. Wu, “Towards scalable 3D anomaly detection and localization: A benchmark via 3D anomaly synthesis and a self-supervised learning network,” in *CVPR*, 2024.
- [44] P. Bergmann and D. Sattlegger, “Anomaly detection in 3D point clouds using deep geometric descriptors,” in *WACV*, 2023.
- [45] V. Zavrtanik, M. Kristan, and D. Skočaj, “Cheating depth: Enhancing 3D surface anomaly detection via depth simulation,” in *WACV*, 2024.
- [46] A. Nekrasov, M. Burdorf, S. Worrall, B. Leibe, and J. S. B. Perez, “Spotting the unexpected (STU): A 3D LiDAR dataset for anomaly segmentation in autonomous driving,” in *CVPR*, 2025.

- [47] P. de Jorge, R. Volpi, P. K. Dokania, P. H. S. Torr, and G. Rogez, "Placing objects in context via inpainting for out-of-distribution segmentation," in *ECCV*, 2024.
- [48] M. Duan *et al.*, "Panoramic out-of-distribution segmentation," *arXiv preprint arXiv:2505.03539*, 2025.
- [49] L. Yang *et al.*, "Depth anything V2," in *NeurIPS*, 2024.
- [50] M. Awad, R. Khanna, M. Awad, and R. Khanna, "Support vector regression," *Efficient Learning Machines: Theories, Concepts, and Applications for Engineers and System Designers*, 2015.
- [51] Y. Duan *et al.*, "Vision-RWKV: Efficient and scalable visual perception with RWKV-like architectures," in *ICLR*, 2025.
- [52] M. Ye, R. Wan, S. Xu, T. Cao, and Q. Chen, "Efficient point cloud segmentation with geometry-aware sparse networks," in *ECCV*, 2022.
- [53] M. Berman, A. R. Triki, and M. B. Blaschko, "The Lovász-Softmax loss: A tractable surrogate for the optimization of the intersection-over-union measure in neural networks," in *CVPR*, 2018.
- [54] J. Mei, Y. Yang, M. Wang, T. Huang, X. Yang, and Y. Liu, "SSC-RS: Elevate LiDAR semantic scene completion with representation separation and BEV fusion," in *IROS*, 2023.